ANALYSIS OF RICE PHENOLOGICAL DIFFERENCES UNDER HEAVY METAL STRESS BASED ON MULTI-SOURCE REMOTE SENSING TIME-SERIES IMAGES

Tianjiao Liu (1)

[1] North China Institute of Aerospace Engineering, 133 Aimin East Road, Guangyang District, Langfang, 065000, Hebei, China
Email: 1226379425@qq.com

KEY WORDS: heavy metal stress; rice; time-series; remote sensing; phenological differences

ABSTRACT: Quickly and accurately monitoring heavy metal pollution have important practical significance. Heavy metal pollution in crops leads to phenological changes, which can be monitored by remote sensing technology. This study focused on investigating rice phenological differences under different heavy metal stress levels using an integrated NDVI (Normalized Difference Vegetation Index) time-series from multi-source remote sensing images. The S-G filtering method was applied to reconstruct time-series data, and phenological metrics were extracted from the reconstructed time-series data of NDVI to investigate the rice phenological differences under mild, moderate and severe stress levels. Results indicated phenological metrics existed differences under different heavy metal stress levels, and metric values under severe stress for presenting rice phenological differences were smaller than the ones under mild stress and moderate stress. This finding demonstrated the superiority of remote sensing phenological information applied to rice heavy metal stress monitoring, which can be a new way to distinguish heavy metal stress in rice.

INTRODUCTION

The research on physiological and ecological effects of heavy metal pollution in rice have shown that heavy metal poisoning can lead to thin plant growth, short leaves, serious yellowing and phenological delay(Wagner, 1993; Wang, 2007; Z, 1992; Zhao, 2011), and phenology is often used as an important indicator of crop yield estimation and field management, the phenological length and the growth rate is of great significance to crop growth simulation(Zhao, 2011; Brown, 2008; Dubovyk, 2016; Menzel, 2000), while the phenological information extracted by remote sensing technology can not only reflect the continuous growth and stress state of rice during the whole growth stage, but also avoid uncertainty of selecting the most sensitive spectral parameters to physiological elements in previous study. Furthermore, the researchers can infer the environmental conditions through the phenological changes of crops, especially the soil(Reed, 1994), which is helpful to study the mechanism of rice poisoned by heavy metals by exploring the relationship between rice phenology and stress. VIs time-series with obvious seasonal rhythm are commonly used for the study of phenology in previous research, and NDVI whose seasonal rhythm comprehensively reflect seasonal variation characteristics of rice can reveal the dynamic state of rice accurately according to the spectral reflectivity characteristic of visible vegetation and near infrared band(Carlson, 1997).

STUDY AREA AND DATA

The study area, ranging between 26°03′–28°01′ N and 112°57′–114°07′ E, is located in the Zhuzhou area, downstream from Xiangjiang in Hunan Province. The long-term discharge of large quantities of industrial wastewater, gases, and residues has contaminated water, soil, and crops in the Xiangjiang watershed with different levels of heavy metals. Many rice fields adjacent to the Xiangjiang watershed in Zhuzhou have become seriously polluted. In the study area, we selected three 1.28 km × 1.28 km rice fields labeled as A, B, and C. They have similar climatic condition and vary in heavy metal stress level. The main type of rice in that area is Boyou 9083. The soil environmental quality standard is used to evaluate the pollution levels (Liu, 2009). The pollution levels for areas A, B and C are categorized as "mild level", "moderate level", and "severe level", respectively. In addition, intensive cultivation patterns were used in all experimental areas to ensure adequate irrigation and sufficient fertilizers in paddy fields without pests, weeds, or other environmental issues.

The remote sensing data collected from June to September in 2013, covering the entire rice growing season in Zhuzhou. Three types of remote sensing images were used for remote sensing phenology, including CCD images of HJ-1A/B, Operational Land Imager (OLI) images of Landsat-8, and Enhanced Thematic Mapper Plus (ETM+) images of Landsat-7. According to the absolute radiation calibration coefficient of HJ-1A/B, released by the China Resources Satellite Application Center in 2013, radiometric calibration and layer stacking were applied to the CCD images. Radiometric calibration and atmospheric correction were also needed for both ETM+ and OLI images. The Fast Line-of-sight Atmospheric Analysis of Spectral Hypercubes (FLAASH) model was used for atmospheric correction in the three types of remote sensing images, and geometric correction was based on CCD images. The corrected root-mean-square error (RMSE) was less than 0.5 pixels. In addition, due to the failure of the Landsat-7 airborne scan line corrector (SLC) in May 2003, gapfill processing was required for the ETM+ images.

METHOD

Creation of Integrated NDVI Time Series

The ordinary least-squares (OLS) model is a primary tool for comparing two datasets and predicting one dataset from another, which by finding an optimal matching function, so that the square sum of the error between the predicted value and the actual value is minimized(Anderson, 2011; Peng, 2013). This study used OLS to build an intercalibration equation of VIs derived from OLI, ETM+ and CCD sensors. We used the OLS method to integrate the three remote sensing datasets and established the ordinary least square fitting equation with NDVI extracted from image pairs of CCD, ETM+ and OLI respectively on the same day, so as to predict the NDVI value of CCD data in other time.

In order to verify the consistency of integrated results, statistical analysis indicators such as agreement coefficient (AC) and mean square difference (MSD) that evaluate the consistency of the two datasets were introduced which can effectively distinguish the systemic and non-systematic differences of two datasets, that is, the closer AC value is to 1, the better consistency is; and MSD can be further decomposed into unsystematic mean product-difference (MPDu) and systematic mean product-difference (MPDs). MPDu which are also used to evaluate the difference

of three kinds of images, that is, the lower these three indexes are, the less difference is.

$$AC = 1 - \frac{\sum_{i=1}^{n}(Xi-Yi)^2}{\sum_{i=1}^{n}(|X-Y|+|Xi-X|)(|X-Y|+|Yi-Y|)} \quad (1)$$

$$MSD = \frac{1}{n}\sum_{i=1}^{n}(Xi - Yi)^2 \quad (2)$$

$$MPD_u = \frac{1}{n}\sum_{i=1}^{n}(|Xi - Zi|)(|Yi - Ci|) \quad (3)$$

$$MPD_s = MSD - MPD_u \quad (4)$$

Where X and Y are NDVI mean values of two kinds of images respectively, Xi and Yi are the NDVI values of each pixel, Zi and Ci are regression analysis values, and n is the number of pixels. Due to the presence of cloud and shadow, the time-series NDVI data still had a lot of noise, so they need to be filtered and reconstructed before application (Hird, 2009; Julien, 2010; Lipovetsky, 2010; Madden, 1978). S-G filter is a weighted average algorithm based on sliding window, which calculates smooth value of fixed number of points near a certain point by the n order fitted polynomial, and it's very important to set the polynomial degree and window size, we obtained the appropriate values through constantly try again(Pan, 2015). S-G filter was applied in this study.

Calculation of Rice Phenological Characteristics under Different Heavy Metal Stress Levels

We extracted critical phenological parameters based on the NDVI time series curve, including Start of Season, End of Season, Length of Season, Base Level, Largest Value and Seasonal Amplitude and Seasonal Integral. Length of season means time from start to end of the season. Base level is given as the average of the left and the right minimum values. Seasonal amplitude describes difference between the maximum value and the base level. Rate of increase or decrease is calculated as the ratio of the difference between the left or right 20% and 80% levels. Seasonal integral means the integral of function describing the season from season start to season end. Reed et al. (Reed, 1994) verified that these metrics may not necessarily correspond directly to conventional, ground-based phenological events, but show strong coincidence with expected phenological characteristics. We chose the length of season, base level, seasonal amplitude, growth rate and seasonal integral as the phenological indicators for further research.

RESULTS

Agreement Evaluation of NDVI Time-Series

A number of rice sample plots were selected from each of the three study areas, some were used to establish the ordinary least squares fitting model, and the other part was used to evaluate the accuracy of the intercalibration results, the function relationships based on NDVI obtained from ETM+, OLI and CCD were established respectively, as shown in Figure 1, it can be seen that NDVI calculated by ETM+ and OLI all have a high correlation with NDVI calculated by CCD, the correlation coefficients acquired in area A with mild pollution are 0.8303 and 0.8484, respectively; the correlation coefficients acquired in area B with moderate pollution are 0.808 and 0.8802, respectively; the correlation coefficients acquired in area C with severe pollution are 0.844 and 0.8582, respectively; and among the three study areas, NDVI calculated by Landsat-8 OLI

had a higher correlation with the NDVI calculated by CCD, which may indicate that compared with ETM+, the sensor parameters of OLI is closer to that of CCD.

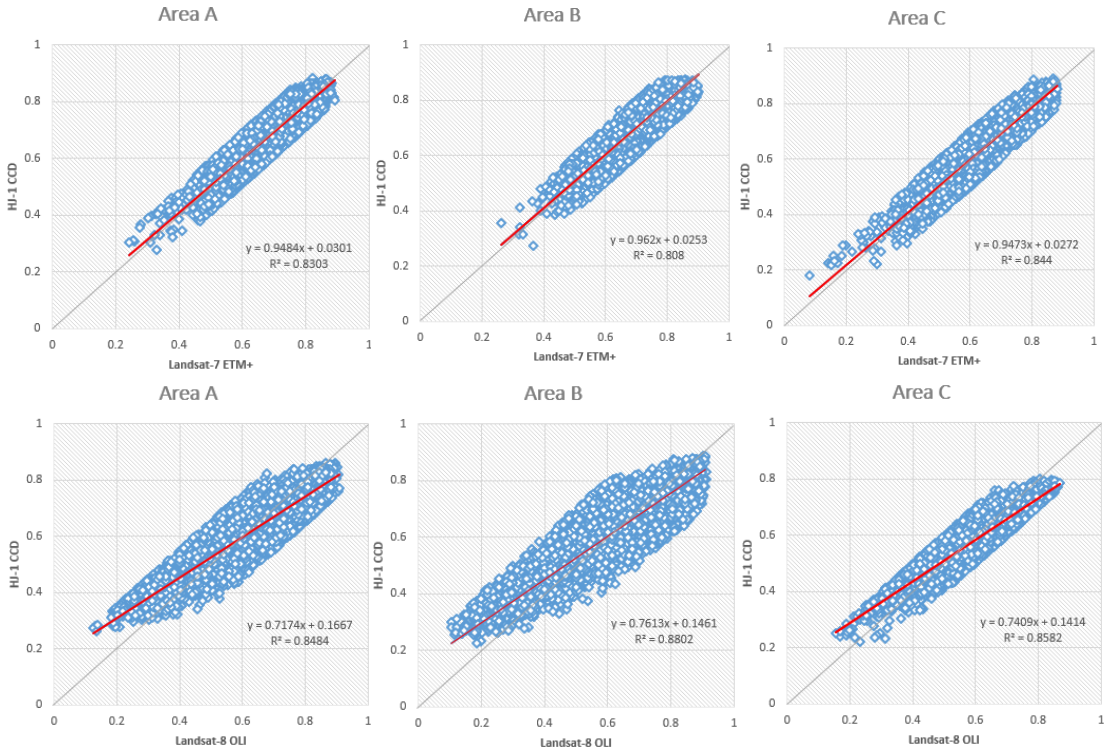

Figure 1. The regression relationship of NDVI calculated by ETM+, OLI and CCD images

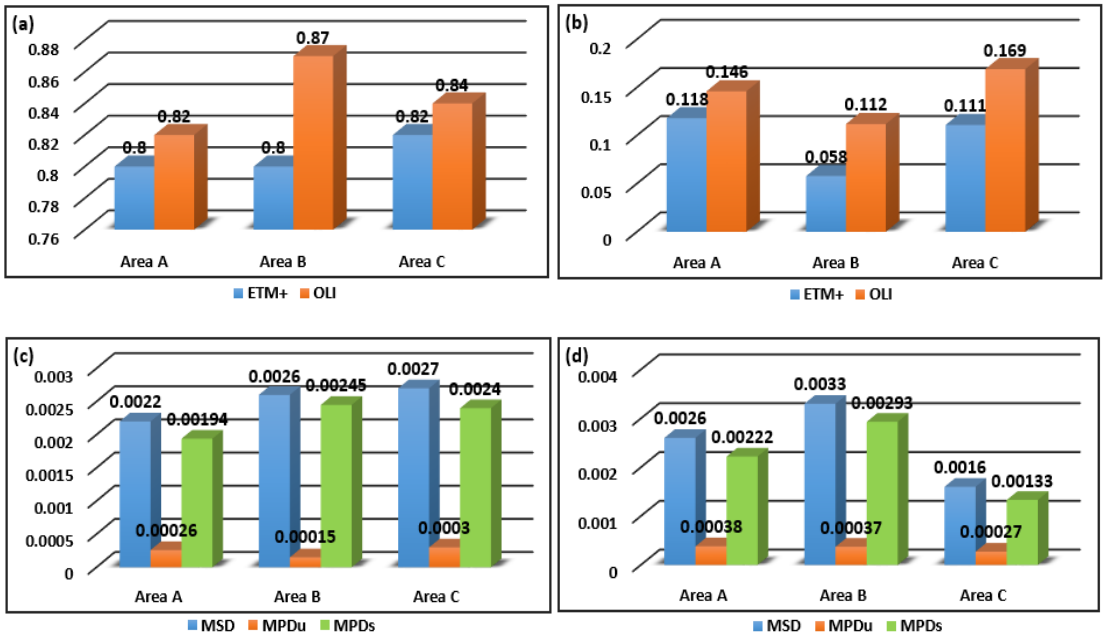

Figure 2. Agreement evaluation of integration results: (a) exhibits the values of agreement coefficient (AC); (b) exhibits the ratio of unsystematic mean product-difference (MPDu) to systematic mean product-difference (MSD); (c) exhibits the values of systematic mean product-difference (MSD), unsystematic mean product-difference (MPDu) and systematic mean product-difference (MPDs) based on CCD and ETM+; and (d) exhibits the values based on CCD and OLI.

The differences between NDVI values acquired from CCD and those obtained from ETM+ and

OLI were compared by calculating the statistical analysis indicators such as AC, MSD, MPDu, MPDs, and MPDu/MSD, as shown in Figure 2. All AC values are close to one, and the AC values based on OLI and CCD are greater than those based on ETM+ and CCD. CCD and OLI may have more consistency compared with ETM+. MSD, MPDu, MPDs, and MPDu/MSD values are all small, meaning the error among the three types of images is relatively small, verifying that integrated NDVI time series derived from CCD, ETM+, and OLI images achieved good results in this study. Additionally, the MPDs values are much higher than the MPDu values for the NDVI of the three datasets, indicating that systematic differences were the primary difference among the three datasets.

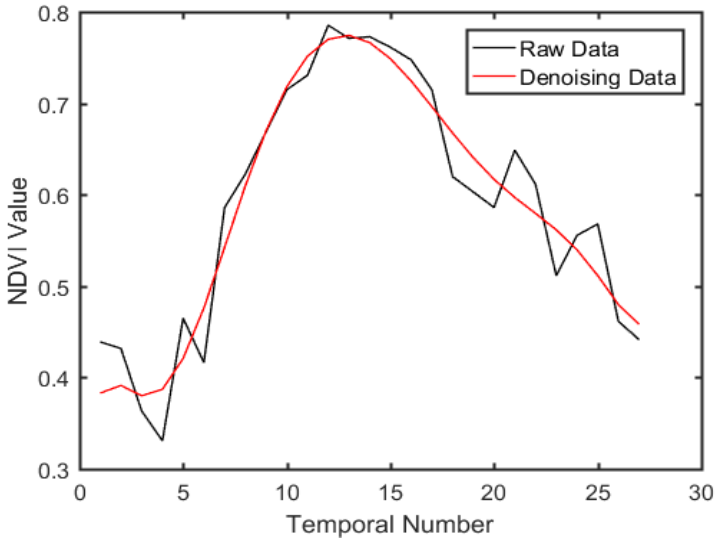

Figure 3. The fitting curve of S-G filter

It can be seen from Figure 3 that Savitzy-Golay filter is closely related to the original data. Statistical analysis indicators such as mean, standard deviation, root mean square error (RMSE) and correlation coefficient (r) were used to further quantitatively evaluate the accuracy of Savitzy-Golay filter, and the values are 0.59, 0.12, 0.06 and 0.88 respectively.

Difference Analysis of Phenological Indicators under Heavy Metal Stress

Five indicators, including seasonal amplitude, base level, growth ratio, length of season, and seasonal integral were calculated in the three experimental areas, as shown in Figure 4. According to statistical analysis, the amplitude range of areas A, B, and C were 0.34–0.59, 0.28–0.48, and 0–0.46, respectively. Area A still had pixel distribution in the range of 0.48–0.59. For area B, 93 pixels were in 0.36–0.46, accounting for 44.5% of the total number of pixels, whereas area C had 58 pixels in this range, accounting for 25.4% of the total number of pixels. Compared with area C, area B had more pixels in this range, displaying the different influences of heavy metal stress on the seasonal amplitude. The base level of areas A, B, and C were distributed within 0.36–0.59, 0.26–0.44, and 0.19–0.41 respectively. Figure 4c shows the discrepancy in the pixel number in each interval among the three experimental regions. The pixels for area A were mainly distributed in the range of 0.44–0.59, whereas no pixels were distribution in this range for areas B and C. The number of pixels in the range of 0.36–0.39 for areas B and C were 46 and 36, accounting for 22.3% and 15.8% of the total number of pixels, respectively. The number of pixels in the range of 0.39–0.41 for areas B and C were 31 and 13, accounting for 14.8% and 6% of the total number of pixels, respectively.

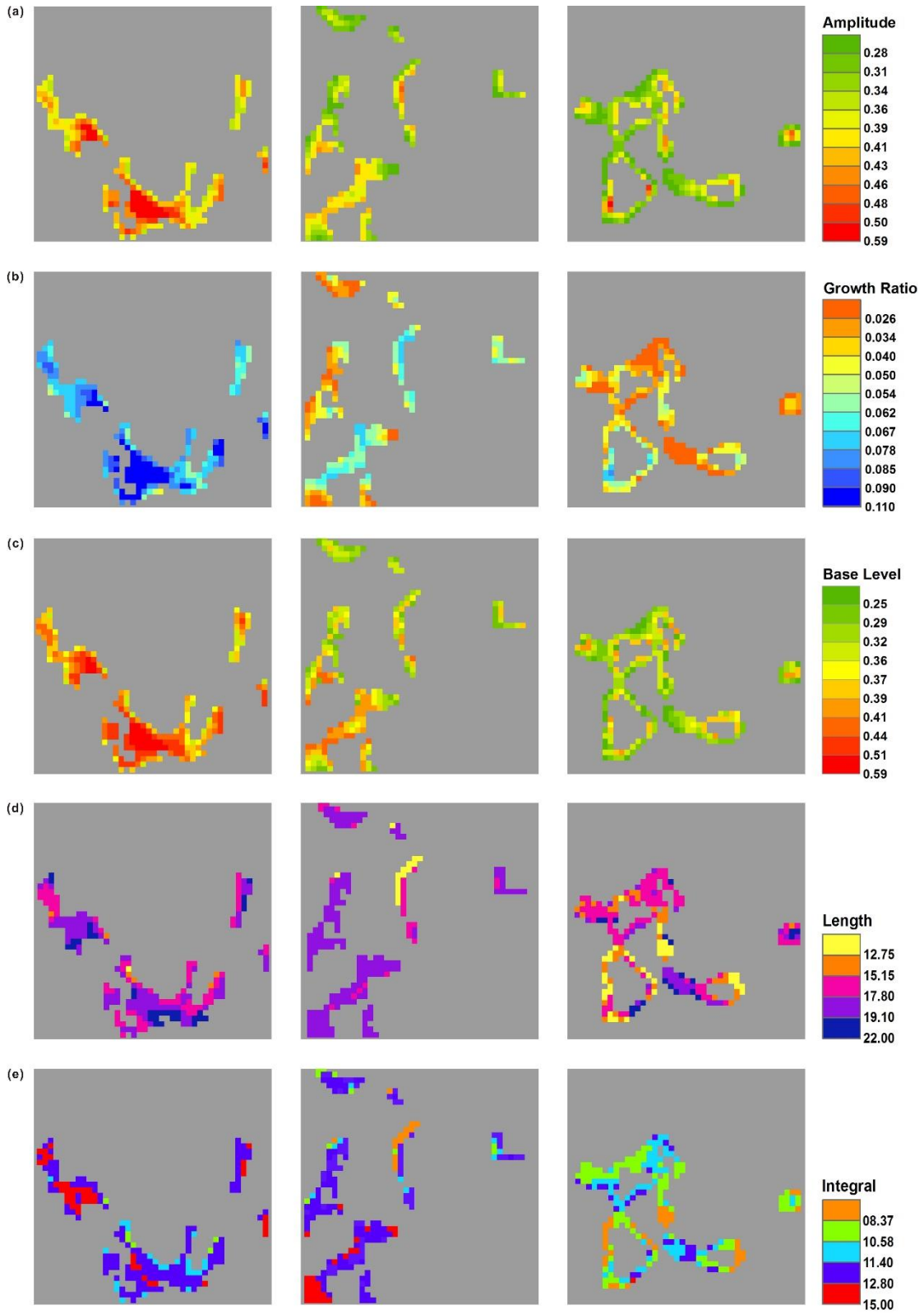

Figure 4. The spatial distribution of five phenological indicators including (a) seasonal amplitude, (b) growth ratio, (c) base level, (d) length of season and (e) seasonal integral for analyzing heavy metal stress levels in rice.

The growth rate of areas A, B, and C were in the range of 0 to 0.11. Figure 4b shows the different heavy metal stress levels according to growth ratio in space. The distribution of rice pixels for area A, ranging from 0.05 to 0.11, was relatively concentrated, whereas the growth rate for areas

B and C were mainly concentrated in 0.026–0.078, with 47.4% and 17% of pixels found in 0.05–0.078 in areas B and C, respectively. The proportion of pixels in area B was much greater than that in area C. The trend in growth rate was consistent with the conclusions obtained in prior studies that heavy metal stress reduced the growth rate of rice, which led to the unfolding of the leaves and the inhibition of radicle growth (Zhao, 2011). The distinction in growth rate was superior to seasonal amplitude. In comparison with the above phenological indicators, the differentiation in length of season was not obvious, as presented in Figure 4d. Length of season had a higher coincidence degree in each division interval, and directly distinguishing the three pollution areas was difficult. In Figure 4e, the number of relatively high values in areas A and B was greater than in area C, which may indicate that area C was most seriously affected by heavy metal stress. However, the distribution of rice pixels in areas A and B were concentrated in the range of 11.4 to 15, and the distinction between A and B was not obvious. In summary, the base level was relatively sensitive to the monitoring of heavy metal stress in the study area, whereas the length of season and the seasonal integral were not sensitive.

DISCUSSION AND CONCLUSIONS

The load parameters of CCD, ETM +, and OLI are generally consistent, having high correlation, and the consistency between the images is close to 0.9, which means we could obtain closer NDVI time series to detect phenological information. The feasibility of multi-source remote sensing data for phenological research was verified. The performance of noise reduction and time-series construction techniques were judged by the ability to reflect the essential shape of the time-series, so that phenological parameters could be accurately extracted (Hird, 2009). Eklundh and Jonsson suggested that the S-G filter is preferable when time series data is used to derive seasonality parameters (Eklundha, 2012). We found that the S-G filter had the great effect on the research area based on characteristic analysis and quantitative statistical analysis. The correlation between the filtered data and the original data was close to 0.9, showing the growth of rice could be truly reflected, which is also consistent with previous conclusions.

We selected length of season, base level, seasonal amplitude, growth ratio, and seasonal integral as phenological indicators. The results showed that these phenological indicators can reflect the heavy metal stress difference to some extent. The results showed that the heavier the heavy metal stress is, the smaller the phenological indicator values would be, which can be used as an important feature to distinguish stress levels. The results can be explained from two aspects: firstly, when the rice is under heavy metal stress, the activity of the enzyme required for chlorophyll formation is inhibited, and chlorophyll content decreased, resulting in chlorosis symptoms in rice (Wagner, 1993; Wang, 2007; Z, 1992; Zhao, 2011), which performed in the NDVI time-series is the reduction of maximum and minimum NDVI values, that may reduce seasonal amplitude, base level, seasonal integral. Secondly, heavy metal stress leads to changes in rice morphology, such as curly leaves and fallen leaves. The rice cannot get enough photosynthetic products due to the reduced LAI. Meanwhile, the transport of photosynthetic products to the organs is hindered, affecting the capacity of organs to transform photosynthetic products into dry matter (Das, 1997), therefore, the growth rate and the length of season may be reduced.

REFERENCES

Anderson, J.H.; Weber, K.T.; Gokhale, B.; Chen, F., 2011. Intercalibration and evaluation of resourcesat-1 and landsat-5 ndvi. Canadian Journal of Remote Sensing, 37, 213-219.
Brown, M.E.; Beurs, K.M.D., 2008. Evaluation of multi-sensor semi-arid crop season parameters based on ndvi and rainfall. Remote Sensing of Environment, 112, 2261-2271.
Carlson, T.N.; Ripley, D.A., 1997. On the relation between ndvi, fractional vegetation cover, and leaf area index. Remote Sensing of Environment, 62, 241-252.
Das, P.; Samantaray, S.; Rout, G.R., 1997. Studies on cadmium toxicity in plants: A review. Environmental Pollution, 98, 29-36.
Dubovyk, O.; Landmann, T.; Dietz, A.; Menz, G., 2016. Quantifying the impacts of environmental factors on vegetation dynamics over climatic and management gradients of central asia. Remote Sensing, 8, 600.
Eklundha, L.; Jönssonb, P., 2012. Timesat 3.1 software manual.
Hird, J.N.; Mcdermid, G.J., 2009. Noise reduction of ndvi time series: An empirical comparison of selected techniques. Remote Sensing of Environment, 113, 248-258.
Julien, Y.; Sobrino, J.A., 2010. Comparison of cloud-reconstruction methods for time series of composite ndvi data. Remote Sensing of Environment, 114, 618-625.
Lipovetsky, S., 2010. Double logistic curve in regression modeling. Journal of Applied Statistics, 37, 1785-1793.
Liu, Y.; Tang, Q.; Bai, Z.; Zhang, X.; Zhang, B., 2009. The resarch of heavy metals pollution in soil based on the connection of geoaccumulation index and nemero index. Chinese Agricultural Science Bulletin.
Madden, H.H., 1978. Comments on the savitzky-golay convolution method for least-squares-fit smoothing and differentiation of digital data. Analytical Chemistry, 50, 1383-1386.
Menzel, A., 2000. Trends in phenological phases in europe between 1951 and 1996. International Journal of Biometeorology, 44, 76-81.
Pan, Z.; Huang, J.; Zhou, Q.; Wang, L.; Cheng, Y.; Zhang, H.; Blackburn, G.A.; Yan, J.; Liu, J., 2015. Mapping crop phenology using ndvi time-series derived from hj-1 a/b data. International Journal of Applied Earth Observation & Geoinformation, 34, 188-197.
Peng, L.; Jiang, L.; Feng, Z., 2013. Cross-comparison of vegetation indices derived from landsat-7 enhanced thematic mapper plus (etm+) and landsat-8 operational land imager (oli) sensors. Remote Sensing, 6, 310-329.
Reed, B.C.; Brown, J.F.; Vanderzee, D.; Loveland, T.R.; Merchant, J.W.; Ohlen, D.O., 1994. Measuring phenological variability from satellite imagery. Journal of Vegetation Science, 5, 703–714.
Wagner, G.J, 1993. Accumulation of cadmium in crop plants and its consequences to human health. Advances in Agronomy, 51, 173-212.
Wang, Q.E.; Zeng, Y.; Li-Mei, L.I, 2007. Advances on the effect of cadmium damage on physiology and ecology of rice. North Rice.
Z, R.; DC, E, 1992. Mechanism of aluminum inhibition of net ca uptake by amaranthus protoplasts. Plant Physiology, 98, 632-638.
Zhao, H.; Yang, Z.; Di, L.; Pei, Z., 2011. Evaluation of temporal resolution effect in remote sensing based crop phenology detection studies. Springer Berlin Heidelberg, 135-150.